



**HAL**  
open science

# Large-strain functional fatigue properties of superelastic metastable $\beta$ titanium and NiTi alloys: A comparative study

L. Héraud, P. Castany, M. F. Ijaz, D. M. Gordin, T. Gloriant

## ► To cite this version:

L. Héraud, P. Castany, M. F. Ijaz, D. M. Gordin, T. Gloriant. Large-strain functional fatigue properties of superelastic metastable  $\beta$  titanium and NiTi alloys: A comparative study. *Journal of Alloys and Compounds*, 2023, 953, pp.170170. 10.1016/j.jallcom.2023.170170 . hal-04123739

**HAL Id: hal-04123739**

**<https://hal.science/hal-04123739>**

Submitted on 9 Jun 2023

**HAL** is a multi-disciplinary open access archive for the deposit and dissemination of scientific research documents, whether they are published or not. The documents may come from teaching and research institutions in France or abroad, or from public or private research centers.

L'archive ouverte pluridisciplinaire **HAL**, est destinée au dépôt et à la diffusion de documents scientifiques de niveau recherche, publiés ou non, émanant des établissements d'enseignement et de recherche français ou étrangers, des laboratoires publics ou privés.

**Large-strain functional fatigue properties of superelastic metastable  $\beta$  titanium and NiTi alloys: A comparative study**

Lorène Héraud<sup>a,1</sup>, Philippe Castany<sup>a,\*</sup>, Muhammad Farzik Ijaz<sup>b,a</sup>, Doina-Margareta Gordin<sup>a</sup>,  
Thierry Gloriant<sup>a</sup>

*<sup>a</sup>Univ Rennes, INSA Rennes, CNRS, ISCR UMR 6226, 35000, Rennes, France*

*<sup>b</sup>Mechanical Engineering Department, College of Engineering, King Saud University, P.O.  
Box 800, Riyadh 11421, Saudi Arabia*

\*Corresponding author: P. Castany; philippe.castany@insa-rennes.fr.

*<sup>1</sup>Present address: Arts et Métiers Institute of Technology, University of Bordeaux, CNRS,  
Bordeaux INP, INRAE, HESAM Université, I2M, Esplanade des Arts et Métiers, 33400  
Talence, France*

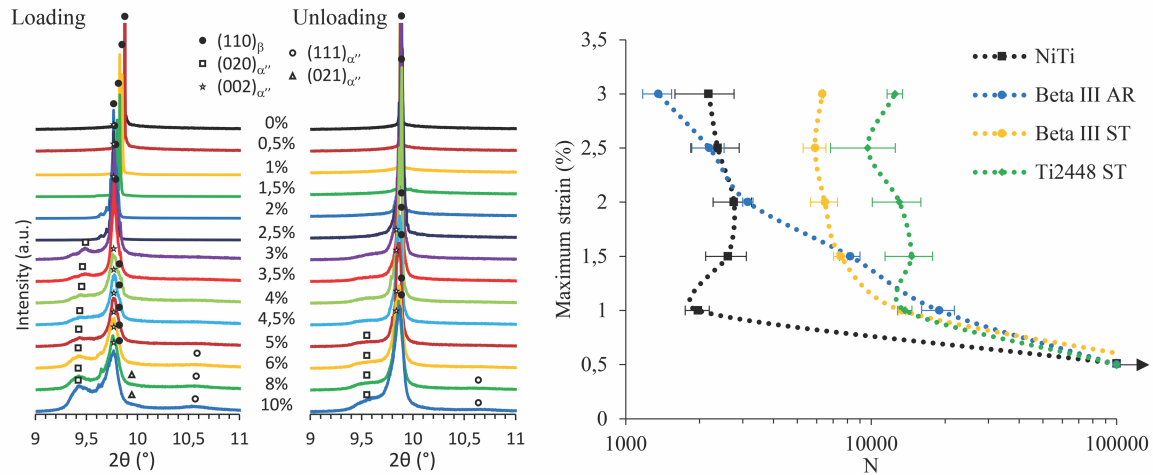
## ABSTRACT

This paper investigates the fatigue behavior of superelastic NiTi and two metastable  $\beta$  titanium alloys - commercial Beta III (Ti-11.5Mo-6Zr-4.5Sn wt.%) and Ti2448 (Ti-24Nb-4Zr-8Sn wt.%) alloys. *In situ* cyclic tensile tests performed under synchrotron X-ray radiation were used to precisely characterize the stress induced martensitic (SIM) transformation occurring in these alloys. For the NiTi alloy, an intermediate B2-R SIM transformation was detected before the B2-B19' SIM transformation and no plastic deformation occurred until failure. All metastable  $\beta$  titanium alloys that were solution-treated before testing underwent a reversible  $\beta$ - $\alpha''$  SIM transformation and plastic deformation prior to failure. Low-cycle strain-controlled fatigue tests were performed in tension-tension strain-controlled mode at 37°C to evaluate large-strain functional fatigue properties. The fatigue life of metastable  $\beta$  titanium alloys was found to be much better than that of NiTi alloy at large applied strains. After a rapid evolution during the first cycles, the mechanical response was found to be constant for NiTi alloy while it evolved continuously for metastable  $\beta$  titanium alloys. In addition, failure occurred suddenly in NiTi, whereas cyclic softening was observed before failure in metastable  $\beta$  titanium alloys. Fatigue properties at higher applied strains are mainly hindered by SIM transformation and defects generated at austenite/martensite interfaces during cycling. This explains why the studied NiTi alloy showed lower fatigue properties than metastable  $\beta$  titanium alloys. In fact, while SIM transformation is homogeneously nucleated in metastable  $\beta$  titanium alloys, SIM transformation is highly localized in NiTi, resulting in higher concentration of defects that promote crack nucleation and, in turn, degrade the functional fatigue properties.

**Keywords** Superelasticity, *In situ* synchrotron XRD, Stress induced martensite, Titanium alloys, Functional fatigue.

## Graphical abstract

### SIM transformation & endurance of metastable $\beta$ titanium alloys vs NiTi



## 1. Introduction

Medical devices such as stents, intravascular guidewires, orthopedic staples or orthodontic archwires require specific properties such as superelasticity or shape memory effect to fulfill their function. Superelasticity is due to a reversible Stress Induced Martensitic (SIM) transformation between an austenitic parent phase and a product phase called martensite. Currently, the main superelastic alloys used for these applications are near-equimolar NiTi alloys which are known for their excellent superelasticity [1]. However, these alloys contain about 50% of nickel, which is known as a toxic and allergenic element [1–4]. On the other hand, superelastic Ni-free metastable  $\beta$  titanium alloys, composed of recognized biocompatible elements have been intensively studied due to their great potential in such medical applications. Many of such alloys such as Ti-Nb [5–17], Ti-Mo [18,19], Ti-Zr [20,21] or recently Ti-Hf

[22,23] based systems have been developed with the aim to improve their superelasticity in order to reach that of NiTi. For example, the Ti-24Nb-4Zr-8Sn (wt.%) alloy (Ti2448 for short) is one of the most studied alloys, showing very interesting properties [8,9,13,14] with a superior biocompatibility [15], but is not yet considered for orthodontics, stents or other medical applications using wires. On the other hand, the commercial Beta III alloy is already used in orthodontics and is an interesting alloy to consider for other medical applications due to its potential superelasticity [24].

However, as in almost all superelastic alloys, martensitic transformation is difficult to characterize because of its reversibility. The occurrence of stress hysteresis and transformation plateau on cyclic tensile response curves can be a signature of the SIM transformation, but both are not well defined in Beta III alloy. Studies of SIM transformation must then be carried out by *in situ* X-ray diffraction, to characterize the phases when the alloy is subjected to stress. Such tensile tests have been performed on Ti based alloys using conventional laboratory XRD equipment [16,17,25]. However, the acquisition time must be fast enough to avoid relaxation of martensite, and the main peaks of the austenite and martensite are very close when using wavelengths of laboratory XRD sources. To overcome these limitations, the use of synchrotron radiation is then increasingly favored [7,13,20,21,23,26–28]. It is worth noting that, although a SIM transformation occurs in both  $\beta$  metastable Ti and NiTi alloys, the phases involved are different: SIM transformation occurs from the  $\beta$  phase (bcc) to the  $\alpha''$  phase (orthorhombic) in Ti alloys [5,13,16,26,27] and from the B2 (cubic) phase to the B19' phase (monoclinic) in NiTi alloys [1,29,30]. An intermediate R phase (trigonal) can also be found in some NiTi alloys [29]. Medical devices, such as stents, are required to withstand high amplitude cyclic loading, yet NiTi alloys are known to exhibit relatively poor fatigue resistance, which is the main issue limiting their applications [31,32]. Subsequently, numerous fatigue studies have been performed on NiTi alloys, most of which being stress-controlled [31,33], bending fatigue [34–

36] or functional fatigue [32,37–39]. All conclude that NiTi alloys show an evolution of mechanical response during cycles with a deterioration of the superelastic recovery. In contrast, very few such studies have been performed on metastable  $\beta$  titanium alloys, with most of them focusing on low amplitudes of deformation [40] or stress-controlled fatigue modes [41,42]. However, for applications requiring high deformation and thin specimen geometry (stents, orthodontic archwires ...), these types of tests are not representative and high deformation (0.5-3%), low cycles and strain-controlled fatigue tests should be performed. For such applications, an original type of fatigue testing has been developed for superelastic NiTi alloys: specimens are subjected to repeated cyclic loading between a maximum applied strain and a minimum stress in order to avoid compression and thus detrimental buckling [16,32,38]. The fatigue behavior of NiTi alloys is then sensitive to the type of loading. Compression phases during tension-compression tests are beneficial for fatigue life because microcracks tend to close, whereas microcracks propagate more easily when specimens are only subjected to tensile stress. A tension-tension test will then be a more severe test than a tension-compression test [43]. Therefore, the present study aims at understanding the strain-controlled fatigue behavior of two metastable  $\beta$  titanium alloys (Beta III and Ti2448) and comparing it with that of NiTi alloy. To discuss and interpret the fatigue results, the SIM transformation taking place in these alloys is also described by *in situ* synchrotron XRD experiments.

## **2. Materials and methods**

### **2.1. Materials and microstructure**

Experiments were conducted using 1.20 mm diameter metallic wires. Beta III wires were purchased from Fort Wayne metals and NiTi wires from Euroflex. The compositions of Beta III and NiTi alloys are Ti-11.5Mo-6Zr-4.5Sn (wt.%) and 56Ni-44Ti (wt.%) respectively. The Ti2448 (Ti-24Nb-4Zr-8Sn wt.%) alloy was elaborated in the laboratory from pure elements

by cold crucible levitation melting [21,22] and cold wire drawn to 1.20 mm wires. After wire drawing, a solution treatment (ST: 900 °C for 30 min followed by water quenching) was performed. Ti2448 alloy was then characterized in this ST state, and NiTi alloy in its as-received state. Beta III alloy was characterized in two states: as received (AR) and after solution treatment (ST) at 950°C for 30 min followed by water quenching. All heat treatments were carried out under high vacuum ( $\sim 10^{-7}$  mbar).

Microstructures were characterized by optical microscopy (Leica microscope). All  $\beta$  titanium specimens were mechanically prepared with SiC papers, “mirror” polished with a colloidal silica suspension and finally etched in a 5% HF, 5% HNO<sub>3</sub>, 90% H<sub>2</sub>O (vol.) solution. Due to its very small grain size, the microstructure of NiTi alloy was observed by Transmission Electron Microscopy (TEM), using a Jeol 2100 machine working with an accelerating voltage of 200 kV. Samples were thinned down by twin-jet electropolishing with a solution composed of 4% (vol.) perchloric acid in methanol at 253 K.

## **2.2. Mechanical properties**

A gauge section was machined from the 1.20 mm diameter wires with a reduced diameter of 0.5 mm and a gauge length of 15 mm. Basic mechanical properties were evaluated by tensile test carried out on an INSTRON ElectroPuls™ E3000 machine. To accurately evaluate the superelasticity, cyclic loading–unloading tensile tests were also performed. These tests consist in loads to a strain value that was incremented by steps of 0.5% and each step was followed by a total release of the stress. All tensile tests were performed at a strain rate of  $10^{-4}$  s<sup>-1</sup>. An extensometer was used to accurately evaluate the strain. At least 3 specimens were used per testing condition.

Fatigue tests were performed on the same testing machine. Specimens were subjected to repeated cyclic loading between a maximum strain and a minimum stress of 1 MPa in order to

avoid compression and buckling. The applied maximum strains were 0.5%; 1%; 1.5%; 2%; 2.5% and 3%. All tests were performed at a frequency of 0.5 Hz and at a constant temperature of 37 °C to fit the service temperature of biomedical devices. Each test is repeated 2 to 3 times to ensure repeatability. The maximum cyclic strain at which the specimen did not fail after  $10^5$  cycles was defined as a run out for such low cycle fatigue tests.

### **2.3. *In situ* synchrotron characterization**

In order to precisely characterize the SIM transformation responsible of superelasticity, *in situ* synchrotron X-ray diffraction (SXR) experiments during cyclic tensile tests were conducted. It allows to determine the phases and their lattice parameters at each step of tensile tests under loading and after stress unloading. The *in situ* SRXD tests were performed on the ID22 beam line at the European Synchrotron Radiation Facility (ESRF, Grenoble, France), equipped with a nine-channel multi-analyzer detector and using a high-energy incident X-ray beam ( $\lambda = 0.040002526$  nm). Diffractograms were acquired over the  $2\theta$  angular range 8–24° with a scanning step of 0.005°. A 5 kN micro-tensile machine was used to conduct the cyclic tensile tests. For Beta III alloy, strain increments were of 0.5% until 5.0%, followed by steps at 6%, 8% and 10%. For NiTi alloy, increments were of 1% until 10% and a last step at 12% of strain. SXR scans were then obtained after each increment for both loading and unloading conditions. Such SXR experiments were previously reported by the authors for the Ti2448 alloy in ST condition [13].

## **3. Results**

### **3.1. Initial microstructure**

Optical micrographs of Beta III AR, ST and Ti2448 ST and bright field TEM image of NiTi alloys are presented in Fig. 1 (a), (b), (c) and (d), respectively. The Beta III AR alloy shows a

deformed microstructure with the presence of numerous twins according to the literature [44,45]. The Beta III ST alloy is composed of large equiaxial  $\beta$  grains, with a diameter about one hundred micrometers. The NiTi alloy has a very fine microstructure, making characterization by optical micrography complicated. The TEM micrograph and its corresponding selected area electron diffraction pattern in Fig.1 (d) show a microstructure composed of B2 equiaxed grains of about 100 nm in diameter.

Fig. 2 shows SXRD patterns of the studied alloys. The Beta III AR, Beta III ST and Ti2448 ST alloys show a full  $\beta$  microstructure (Fig. 2 (a, b and c)). One can notice that the diffracted peaks are wider for Beta III AR alloy due to its deformed state. The SXRD pattern of the NiTi alloy in Fig. 2 (d) confirms the full B2 microstructure. Calculated austenitic  $\beta$  lattice parameters of Beta III AR, ST and Ti2448 ST alloys are respectively 0.32840 nm, 0.32740 nm and 0.32988 nm. The austenitic B2 lattice parameter of NiTi alloy is evaluated at 0.30141 nm.

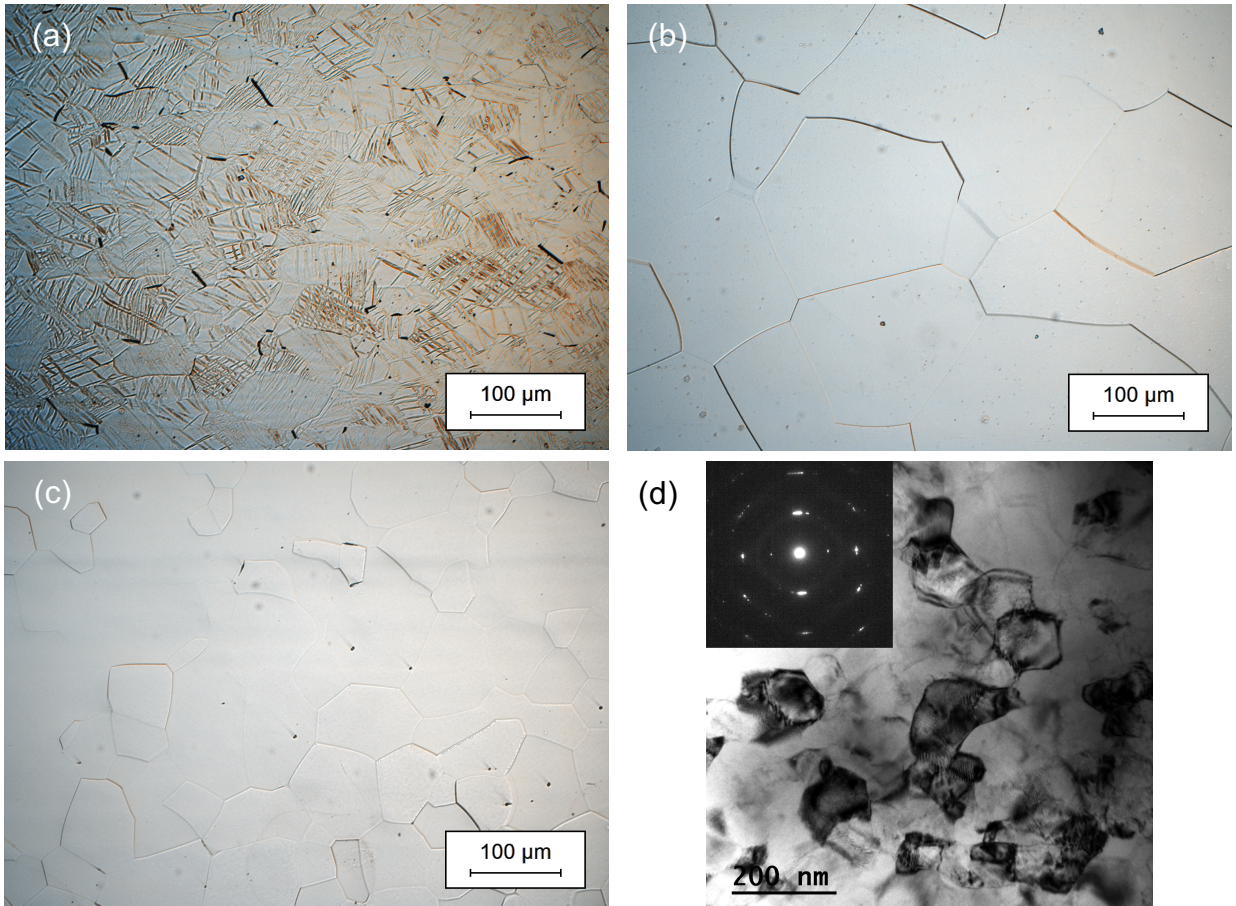


*Fig. 1 - Optical micrographs of the Beta III AR (a) and ST (b); Ti2448 ST (c); and bright field TEM image of NiTi alloy and its diffraction pattern (d).*

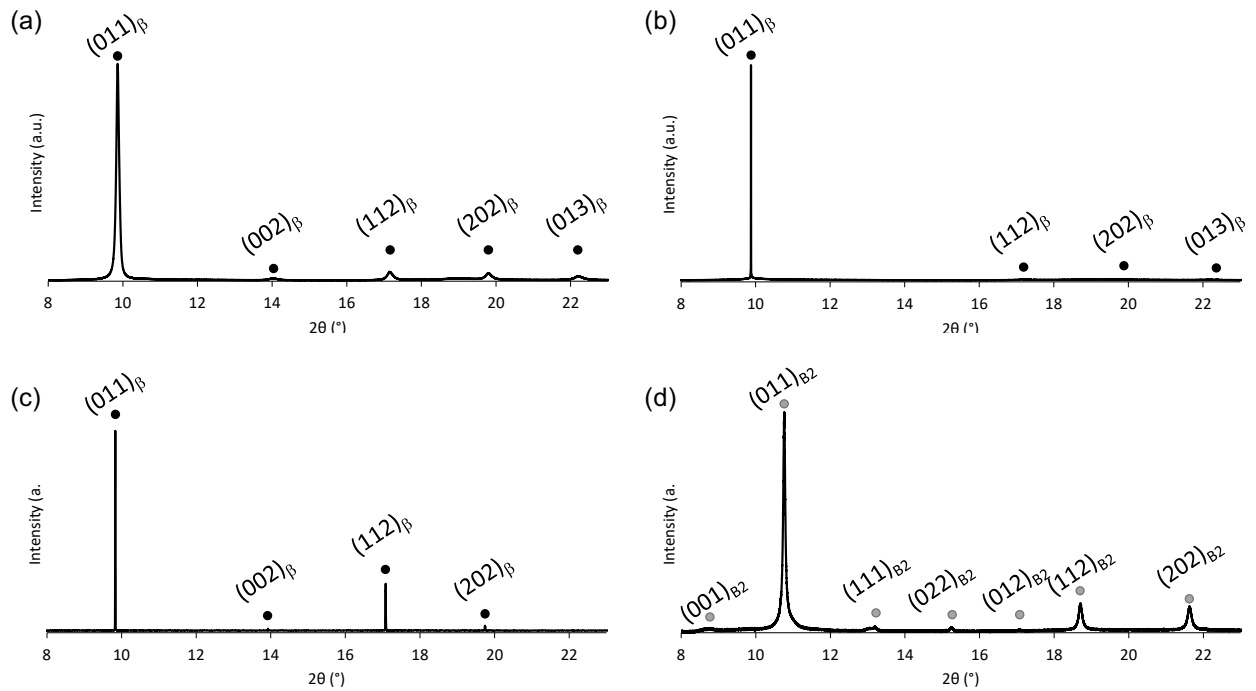


Fig. 2 - SXR D patterns of the Beta III AR (a), Beta III ST (b), Ti2448 ST (c) and NiTi (d) alloys.

### 3.2. Mechanical properties

Mechanical properties were evaluated from conventional tensile curves as plotted in Fig. 3, and are summarized in Table 1 with mean values and standard deviations for each parameter. The Beta III AR and the NiTi alloys show ultimate tensile strength (UTS) higher than 1000 MPa, while the Beta III ST and Ti2448 ST alloys have lower and similar UTS of 700 MPa. However, while Beta III AR alloy breaks at low deformation (about 3-4 %), the Beta III ST alloy shows a good elongation at failure of more than 14 %. The Beta III AR and ST alloys do not exhibit the double yielding behavior observed in Ti2448 ST. Beta III ST and Ti2448 ST alloys have a low Young's modulus, which is appreciated in biomedical applications such as prosthesis or dentistry [46,47]. The NiTi alloy shows good elongation at failure (about 10.5%) but one can notice that there is very few plasticity, with failure occurring just after the elastic deformation of stress-induced martensite. Its high elongation at failure is then mainly due to its large

superelasticity as shown by the 6% long martensitic transformation plateau, starting from about 1% of strain.

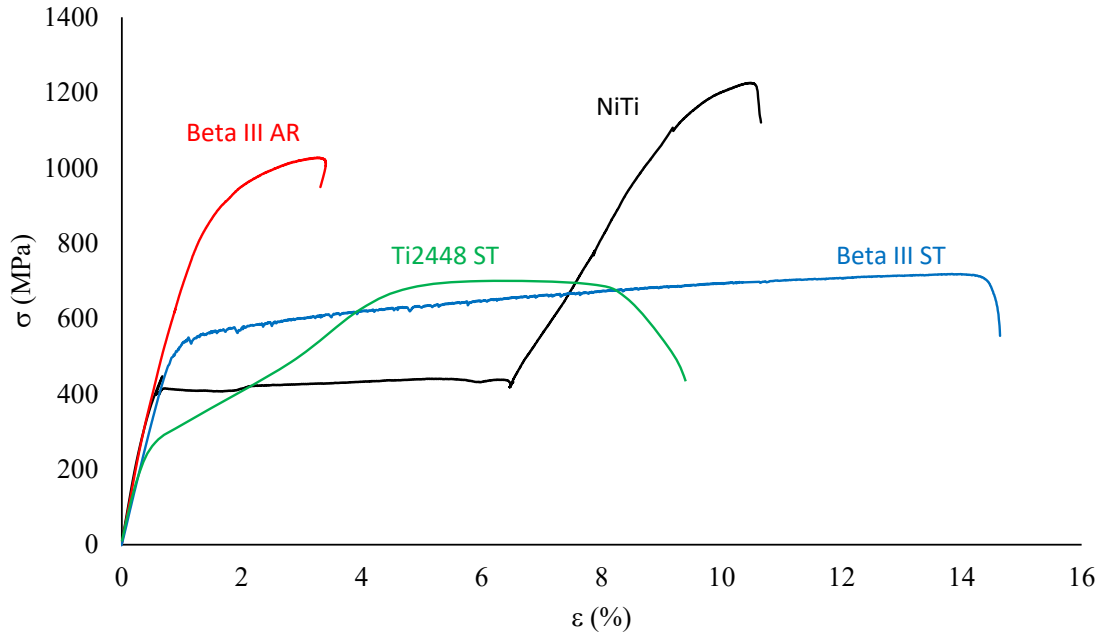


Fig. 3 - Conventional tensile stress–strain curves of Beta III AR, Beta III ST, Ti2448 ST and NiTi alloys at room temperature.

Table 1. Mechanical characteristics of investigated alloys: Elongation at failure ( $A$ ), ultimate tensile strength (UTS), Young's modulus ( $E$ ), maximum recoverable strain ( $\epsilon_{rec}$ ) and residual strain after 2% of applied strain ( $\epsilon_{res2\%}$ ); Standard deviations of  $\epsilon_{rec}$  and  $\epsilon_{res2\%}$  are lower than 0.1%.

Alloy	$A$ (%)	UTS (MPa)	$E$ (GPa)	$\epsilon_{rec}$ %	$\epsilon_{res2\%}$ %
Beta III AR	$3.7 \pm 0.4$	$1013 \pm 15$	$81 \pm 10$	1.9	0.4
Beta III ST	$14.0 \pm 0.5$	$683 \pm 18$	$66 \pm 6$	2.0	0.9
Ti2448 ST	$9.3 \pm 0.7$	$697 \pm 5$	$59 \pm 4$	1.75	0.4
NiTi	$10.6 \pm 0.6$	$1225 \pm 6$	$81 \pm 11$	9.5	0.05

In order to assess the potential superelasticity of all alloys and their recoverable strain, cyclic tensile tests were conducted (Fig. 4). One can notice the appearance of stress hysteresis for all

alloys and particularly for Ti2448 ST and NiTi alloys, which is characteristic of the occurrence of a SIM transformation. In the Beta III AR alloy, the hysteresis is relatively narrow but allows a recoverable strain of 1.9%. In the Beta III ST alloy, an initial accumulation of the residual strain is observed from the first cycles and the hysteresis becomes more important with the increase of the applied strain. In Ti2448 ST alloy, a transformation plateau is detected and the double yielding behavior is observed from 1% to about 4% strain. The main difference between Beta III alloys and Ti2448 ST is that, in Ti2448 ST, the recoverable strain in the first cycles is mainly due to the SIM transformation, occurring at lower stress without much plasticity. In Beta III alloys, the recovered strain is initially mainly due to conventional elasticity because of a combination of high yield strength and low Young's modulus, while the proportion of recovered strain due to the SIM transformation increases with applied deformation, along with the plastic deformation of the alloys. The NiTi alloy shows a larger recoverable strain with a flat transformation plateau. Hysteresis loops are wider due to the difference between the SIM transformation stress and the reverse transformation stress. Up to 8% of applied strain, no significant residual deformation is observed after unloading. For higher applied strains, residual deformation appears and the maximum recoverable strain is obtained for 10% of applied strain with a recoverable strain of 9.5% and a residual strain of 0.5% after unloading. However, unlike Beta III and Ti2448 ST alloys, failure happens abruptly in NiTi alloy, without evidence of plastic deformation.

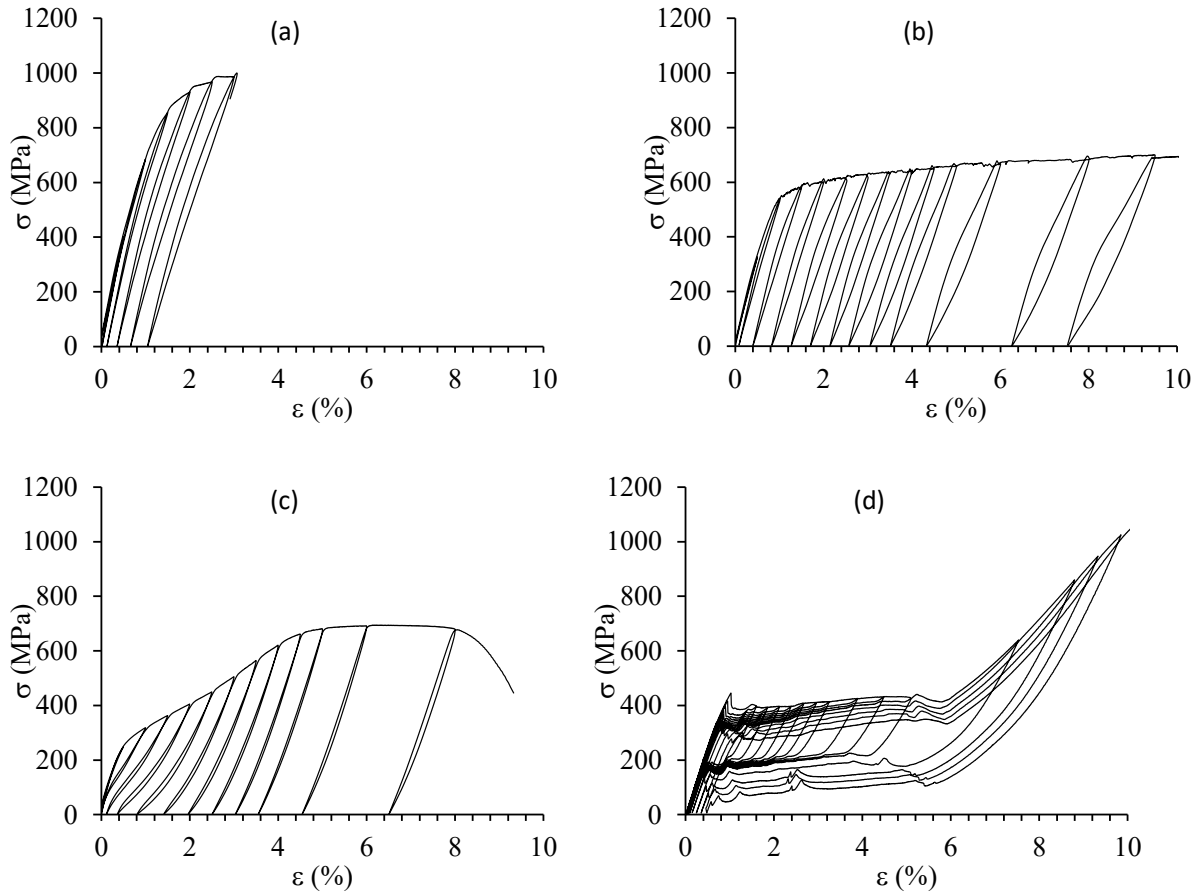


Fig. 4 - Cyclic tensile stress–strain curves of Beta III AR (a), Beta III ST (b), Ti2448 ST (c) and NiTi (d) alloys.

### 3.3. *In situ* SXRD characterization

All alloys were investigated in order to characterize the martensitic transformation responsible for their superelasticity. For Beta III alloy, it is particularly difficult to confirm the occurrence of martensitic transformation only through cyclic tensile curves, that is why *in situ* cyclic tensile tests under SRXD were conducted. Supplementary material (Fig. S1) allows to have an overlook on the complete diffraction patterns of all alloys in their original state, under the greatest achieved strain and after the final release of the stress. Occurrence of SIM transformation is obvious for all alloys when comparing initial SXRD patterns and final SXRD patterns under stress. The comparison with SXRD patterns after unloading also shows a clear reversibility of SIM transformation for all alloys. In order to better characterize SIM

transformation, an enlargement of diffraction patterns obtained under load and after each discharge for each step of cyclic tensile tests is shown around the main peaks of each phase ( $9^{\circ}$ - $11^{\circ}$   $2\theta$  range) in the Fig. 5(a), (b) and (c) for Beta III AR, ST and NiTi alloys, respectively. Results of the Ti2448 ST alloy were previously reported [13] and will not be presented in the present paper. It was shown that in Ti2448 ST the SIM transformation starts at 1% of applied strain and that nearly all of the initial  $\beta$  phase is transformed at around 4% of applied strain.

In Beta III alloys, the main austenitic peak  $(110)_{\beta}$  shifts to smaller angles as the deformation increases (Fig. 5 (a) and (b)), emphasizing the elastic deformation of austenite. In Beta III AR alloy, from 1% of strain (respectively 2.5% for Beta III ST alloy) the intensity of austenitic peak decreases gradually and new peaks appear becoming more intense as the strain increases. Those peaks are due to the appearance of  $\alpha''$  martensite, confirming the occurrence of SIM transformation in Beta III alloys. Once stress is released, intensity of martensitic peaks decreases, or even completely disappears at small applied deformations, showing a full reversibility of the transformation. However, after high deformation, peaks of martensite are still visible in the unloaded state, indicating the presence of stabilized residual  $\alpha''$  phase.

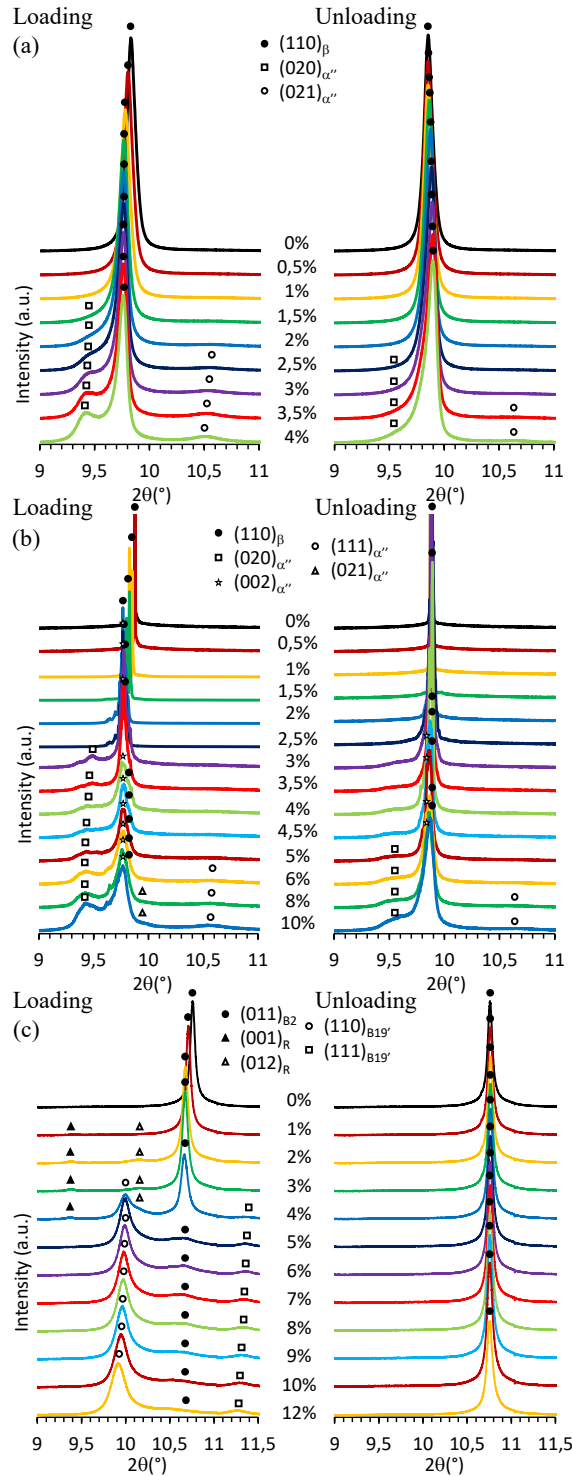


Fig. 5 - SXR D patterns zoomed around the main austenitic peak acquired during in situ cyclic tensile tests under loading (left) and after unloading (right) for the Beta III AR (a), Beta III ST (b) and NiTi (c) alloys; the corresponding applied strain is indicated next to each pattern.

Fig.5 (c) displays the evolution of SXR D patterns of NiTi alloy during cyclic tensile test. In the initial state, the alloy is only composed of B2 austenite. When the applied strain increases, the

B2 austenitic peak shifts to smaller angles and its intensity decreases progressively. From 1% strain, new peaks appear, corresponding to the intermediate R phase. Peaks due to B19' martensite appear from 4% strain, and R phase is no longer observable from 5% strain. It is also interesting to notice that after all stages of deformation, SXR patterns obtained after unloading only consist of austenitic B2 peaks. The SIM transformation is then totally recoverable after any applied strain level in this alloy. This late appearance of B19' in SXR patterns while the stress plateau starts from 1% strain in the tensile test can be explained by the localization of SIM transformation in NiTi alloys. Indeed, it was reported that SIM transformation in NiTi alloys is highly localized in Lüders bands [48–50]. In the present study, the SIM transformation is actually initiated from 1% strain in the specimen gauge section as demonstrated by the transformation plateau in the tensile curve (Fig 2). However, the initiation zone is far from the volume analyzed during SXR experiment, and B19' martensite begins to be detected when the Lüders bands propagate up to the diffracting volume at 4% of applied strain. Moreover, this study proves the non-localized appearance of the intermediate B2-R SIM transformation in the gauge volume, while the B2-B19' SIMT is locally occurring in Lüders bands.

### **3.4. Evolution of lattice parameters**

Evolution of the lattice parameters of austenite and martensite in Beta III AR and ST alloys, evaluated in loading condition, is represented according to the applied strain in Fig. 6. For Beta III alloys, values of lattice parameters of martensite after the final discharge of the stress are represented in Fig. 6, at 0% strain. The  $a_{\beta}$  parameter varies linearly for both conditions up to 2% strain, indicating that the austenite elastically deforms. The austenite lattice parameter then stabilizes when this phase reaches its elastic limit. Some martensitic peaks appear at small deformation in SXR patterns (Fig. 5), but their number is initially too low to calculate lattice parameters. Consequently, martensitic parameters can be calculated for Beta III AR and ST

alloys respectively from 1% and 2.5% deformation. In Beta III alloys, the parameter  $a_{\alpha'}$  slightly fluctuates without much evolution. The  $c_{\alpha'}$  parameter appears also relatively constant regardless of the applied strain. The  $b_{\alpha'}$  parameter increases linearly and stabilizes at 2% strain for the Beta III AR and at 5% for Beta III ST alloy. In both Beta III AR and ST alloys, deformation seems therefore accommodated first by the elastic deformation of the austenite, then by the SIM transformation and by the elastic deformation of the martensite, essentially accommodated along the b axis as previously reported in some Ti-Nb alloys [27]. The alloys are then plastically deformed until failure. The previously reported sequence of deformation of Ti2448 ST alloy is similar [13].

The lattice parameters of NiTi alloy are displayed in Fig.7. During the tensile test, the B2 austenite first deforms elastically up to 2% strain. From 1% strain, the R phase is stress-induced and deforms elastically up to 4% strain. B19' phase then forms from 2% deformation from B2 and R phases, corresponding to the beginning of the SIM transformation plateau observed in the tensile curve Fig. 4 (d). Its lattice parameters are calculated from 5% and increase up to the end of the tensile test. B19' martensite is then elastically deformed during the whole test until failure without any stabilization confirming the absence of any plastic deformation in this alloy.

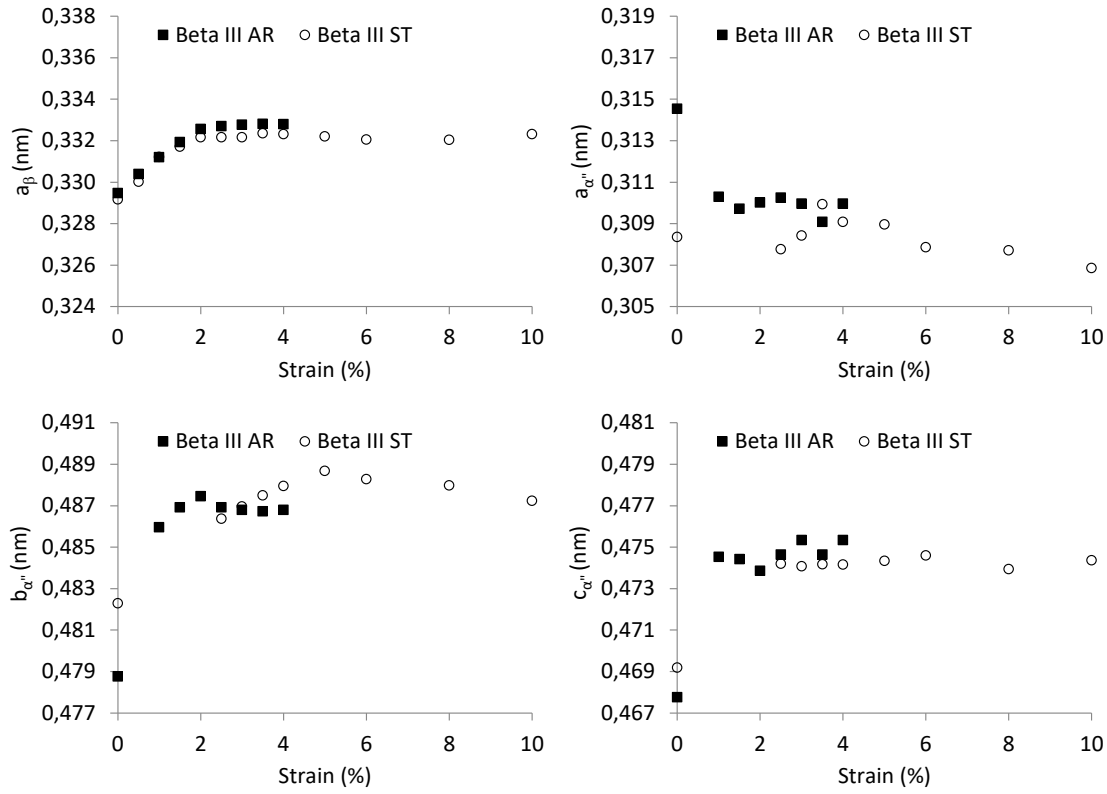


Fig. 6 - Evolution of lattice parameters of  $\beta$  austenitic and  $\alpha''$  martensitic phases as a function of applied strain during in situ tensile tests for both Beta III AR (black squares) and Beta III ST (open circles).

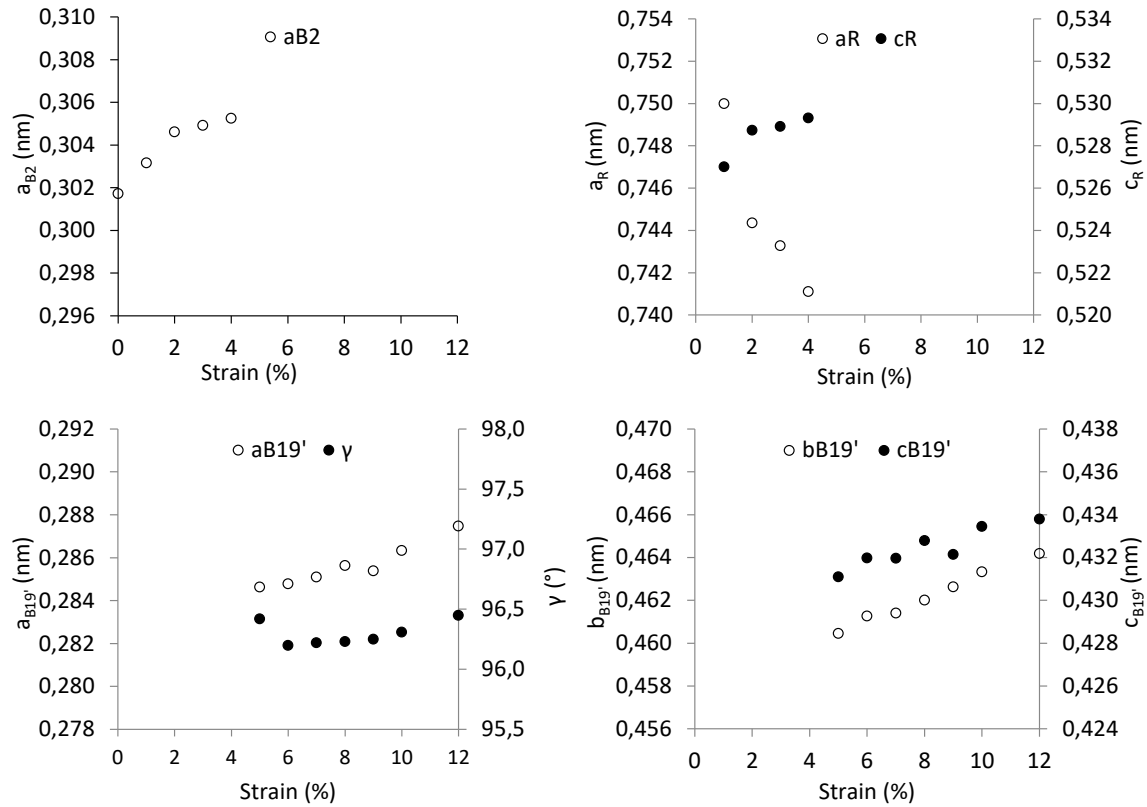


Fig. 7 - Evolution of lattice parameters of B2 austenitic, R and B19' martensitic phases as a function of applied strain during in situ tensile tests for NiTi alloy.

### 3.5. Fatigue

A low cycle fatigue strain-life curve is drawn in Fig. 8 representing the number of cycles to failure ( $N$ ), i.e. the number of cycles until failure of the specimen, of each alloy as a function of the applied strain. NiTi alloy has a relatively constant and short fatigue life from 1.5% to 3% of applied strain. One can notice a decrease in number of cycles to failure for the 1% applied strain condition. This phenomenon appears in the domain of existence of R phase according to tensile tests carried out in this study and to literature [51]. At 0.5% applied strain, the alloy does not undergo SIM transformation and can be deformed during  $10^5$  cycles without failure. Thus, the appearance of SIM transformation seems to deteriorate the fatigue life of NiTi alloy, with a more detrimental effect for the B2-R than for the B2-B19' SIM transformation. Beta III AR and NiTi alloys behave similarly for high maximum applied strain ( $> 2\%$ ) with very similar fatigue life. However, in Beta III AR the number of cycles to failure continuously increases with the decrease of applied strain and shows better fatigue life than NiTi alloy below 2% of maximum applied strain. As for NiTi, this alloy endures  $10^5$  cycles without failure at 0.5% strain, but the number of cycles to failure at 1% strain is higher by more than an order of magnitude. Beta III ST and Ti2448 ST alloys have a similar behavior with superior fatigue resistance, reaching at least three times the fatigue life of NiTi at high applied strain ( $> 1.5\%$ ). The Ti2448 ST alloy exhibits the best fatigue resistance with an increase of one order of magnitude compared to the NiTi alloy. From 1.5% applied strain, the fatigue life of these ST alloys is stable.

In these alloys the appearance of the martensitic transformation seems to have a dominating role on the fatigue life, as was the case for NiTi alloy. As in the previous alloys, no failure is observed for very low applied strain (0.5%).

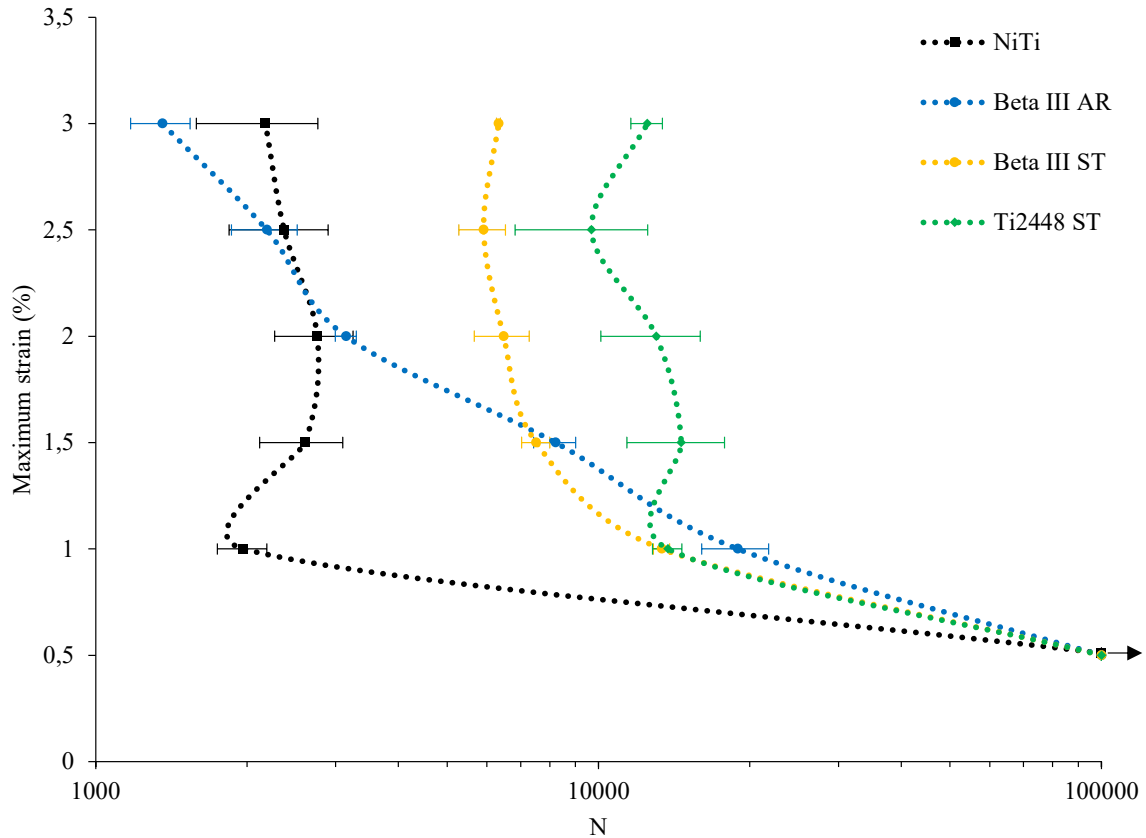


Fig. 8 - Large-strain fatigue curves of Beta III AR, Beta III ST, Ti2448 ST and NiTi alloys for strain-controlled tests. Dashed lines are only guide for the reader. The black arrow represents the run out ( $10^5$  cycles without failure).

Fig. 9 shows the evolution of residual strain and maximum stress during cycles for each maximum applied strain for Beta III AR, Beta III ST, Ti2448 ST and NiTi alloys. In Beta III alloys, residual strains increase during the first cycles and, from about 10 cycles, show a stable mechanical response (Fig. 9a-b). In these alloys a rapid increase in residual strain and a decrease in stress is observed in the last cycles before failure. This reflects a softening of the material and a ductile fatigue failure, allowing to anticipate this fatigue failure.

Ti2448 ST alloy has a different behavior with a continuous decrease of maximum stress with cycles (Fig. 9c). Up to 2.5% applied strain, the first hundred cycles present a slow accumulation of residual strain followed by a significant increase without stabilization until failure. A rapid increase of residual strain accumulation rate is also visible before failure on the curves acquired

from 1.5 to 2.5% of maximum applied strain.

In NiTi alloy, the residual strain increases rapidly during the first tens of cycles and then stabilizes up to failure. At 0.5% strain, SIM transformation does not happen and only elastic deformation occurs. From 1% strain, the maximum stress is rather insensitive to the applied strain and corresponds to the SIM transformation stress plateau (550-650 MPa). Residual strain and maximum stress do not show any variation before failure. This alloy does not present softening, making its fatigue failure difficult to predict.

Representative examples of the evolution of the mechanical response during cycles are given in Fig. 10 for Beta III AR (a) and ST (b), Ti2448 ST (c) and NiTi (d) for fatigue tests at 3% of applied strain until failure. The superelasticity of NiTi and Ti2448 ST alloys deteriorates during cycles. NiTi alloy, however, stabilizes after 100 cycles and breaks shortly after 1500 cycles without change in its mechanical response. The Ti2448 ST alloy does not stabilize and its behavior evolves continuously with cycles up to over 10000 cycles. Its apparent elastic modulus, i.e. the slope of the curve, continuously changes, most probably due to an increasing amount of martensite. The Beta III AR and ST alloys show a fairly stable response during cycles with narrow hysteresis. During the last cycles, a significant softening occurs before breaking. For the Beta III ST and Ti2448 ST alloys, the number of cycles to failure are far greater than the ones of NiTi and Beta III AR alloys at 3 % strain.

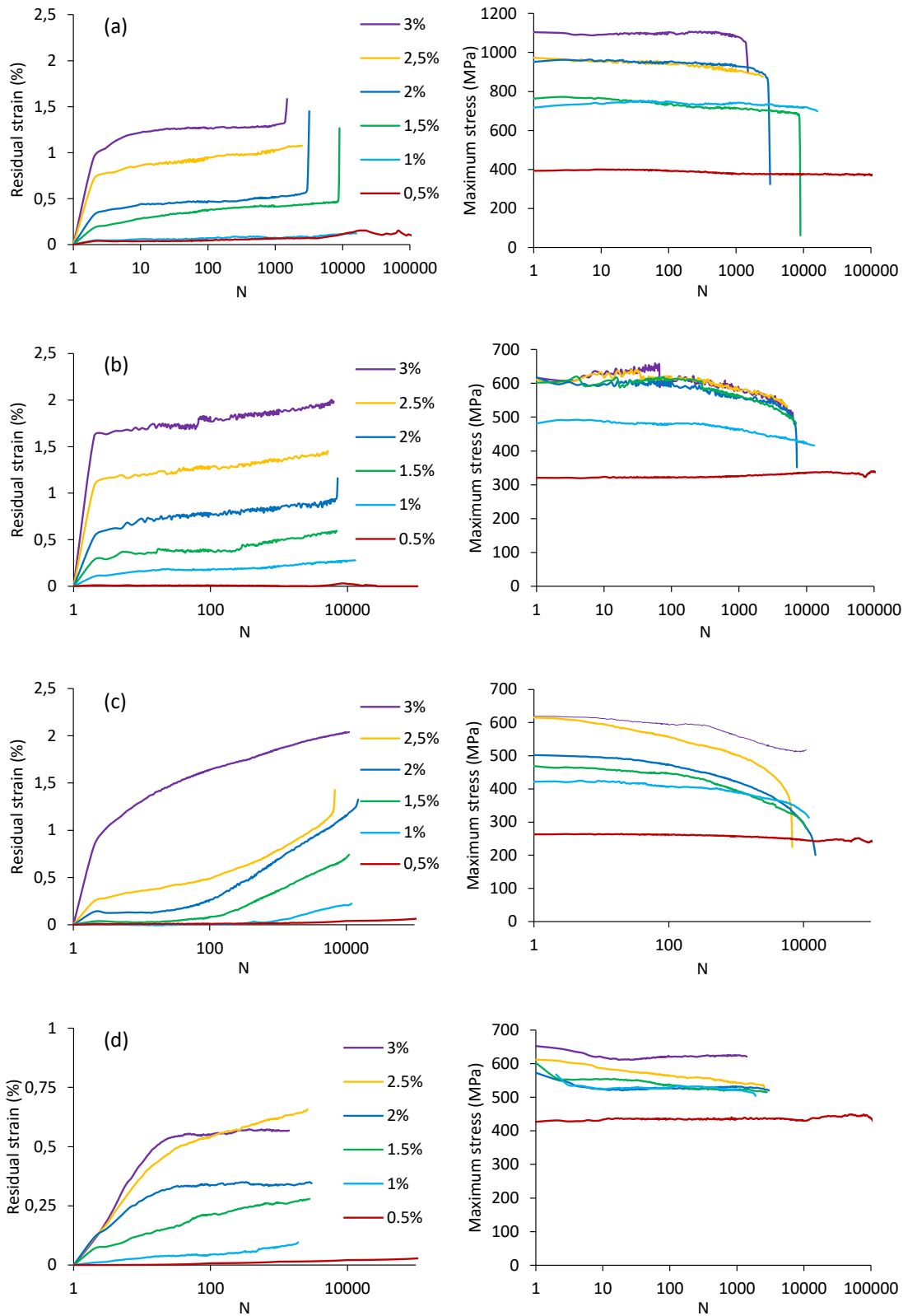


Fig. 9 - Evolution of residual strain and maximum stress with cycles for each level of maximum applied strain for Beta III AR (a), Beta III ST (b), Ti2448 ST (c) and NiTi (d) alloys.

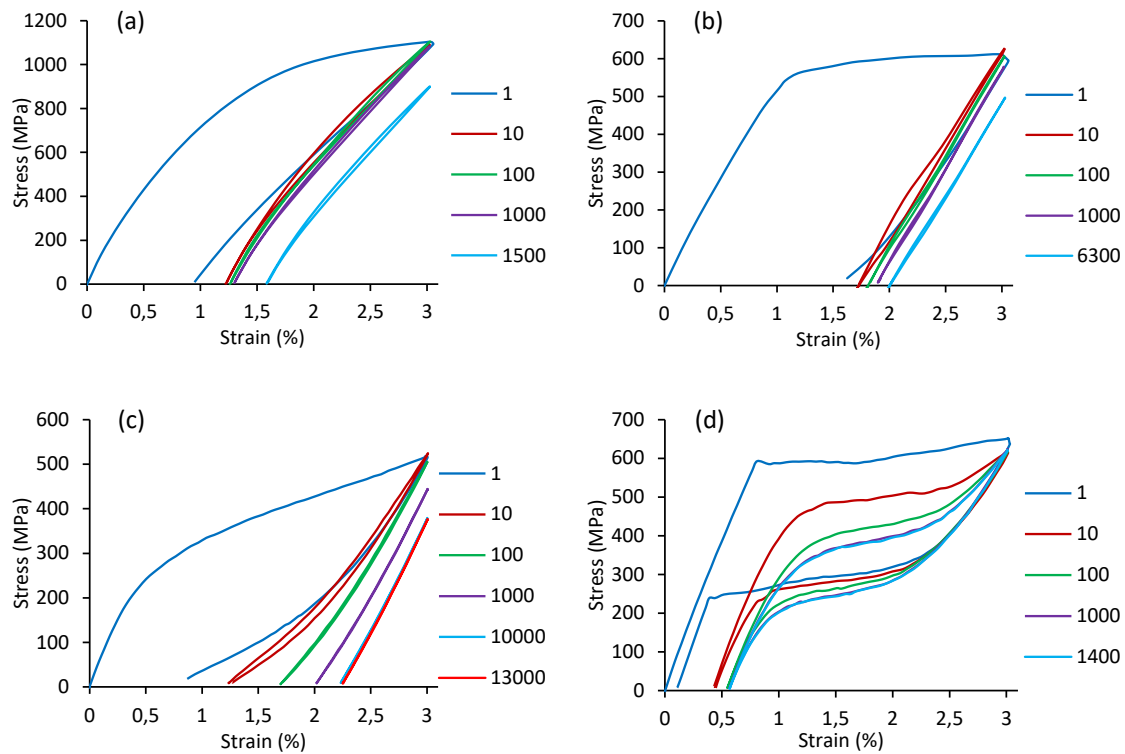


Fig. 10 - Evolution of mechanical response with cycles during 3% strain fatigue test for Beta III AR (a) and ST (b), Ti2448 ST (c) and NiTi (d) alloys.

## 4. Discussion

### 4.1. SIM transformation

The Beta III ST alloy shows a remarkable mechanical behavior with an obvious increase of the hysteresis area with increasing applied strain (Fig. 4b). This indicates that reversible SIM transformation is more frequent as the applied strain increases, as clearly shown by the SXRD results (Fig. 5b). This behavior differs from classical superelastic metastable  $\beta$  titanium alloys which exhibit a clear double yielding behavior with an associated stress plateau [5,13,20–23,26]. However, the activation of SIM transformation during the plastic deformation stage has been observed in alloys with Transformation Induced Plasticity (TRIP) effect, but generally without reversibility [19,52,53]. The present Beta III ST alloy then behaves as a superelastic alloy without double yielding, with a SIM transformation occurring simultaneously with other

plastic deformation mechanisms. Such a peculiar superelastic behavior has already been reported for Ti-24Nb-0.5O (at.%) alloy [27]. One explanation for the increase of SIM transformation with applied strain could be twinning, which is a common deformation mechanism in metastable  $\beta$  alloys [52–55]. Indeed, recent research shows that SIM transformation occurs only within twins in some TRIP alloys [56]. This phenomenon may also occur in the present Beta III ST alloy and may explain the increasing amount of SIM transformation with increasing applied strain.

The Beta III alloy was previously analyzed by *in situ* SXRD during a tensile test by Cai et al. [57] in an annealed condition close to the present ST condition. The occurrence of a reversible SIM transformation was also reported for applied strains of 4%, 5% and 8%, but characterization at lower strains was not performed. This previous study is consistent with the present work of the authors but emphasizes the absence of SIM transformation in the early stage of deformation and its peculiar superelastic behavior.

In contrast to the Beta III alloy, both Ti2448 ST [13] and NiTi (Fig. 4d) alloys exhibit a more classical SIM transformation with a double yielding behavior and a stress plateau. The main difference is that in the NiTi alloy the SIM transformation occurs until failure of the specimen, i.e. without any plastic deformation, while the Ti2448 ST shows a decrease in superelasticity when plastic deformation occurs.

## **4.2. Deformation sequence**

The deformation sequence for all alloys can be established from tensile tests and SXRD results. In Beta III alloys, the  $\beta$  austenite first undergoes a large elastic deformation. Then, although the tensile curves do not show double yielding behavior, the SIM transformation occurs together with the plastic deformation. In Beta III AR alloy, the elastic deformation of martensite is limited, then both martensite and residual austenite deform plastically until fracture. The case

of the Beta III ST alloy is different: SIM transformation occurs simultaneously with plastic deformation of  $\beta$  phase and the contribution of SIM transformation to the total deformation increases with the applied strain. Elastic deformation of martensite occurs up to about 5% of applied strain; after which both phases undergo plastic deformation.

As previously reported [13], SIM transformation is the main deformation mechanism that occurs after the elastic deformation of  $\beta$  phase in the Ti2448 ST alloy. Martensite is then elastically deformed to an applied strain of 5% and is finally plastically deformed to failure.

NiTi alloy exhibits an almost similar sequence of deformation but with two major differences, namely the presence of an intermediate SIM transformation and the absence of plastic deformation. After elastic deformation of B2 austenite, the intermediate B2-R SIM transformation first occurs homogeneously in the applied deformation range of 1% to 2%. From 1% to 4% strain, B2 phase transforms to B19' martensite in Lüders bands, while the R phase is elastically deformed. The three phases then coexist. From 5% strain, the R phase is no longer observable and the B2-B19' SIM transformation becomes the only deformation mechanism. From 6% of applied strain and until the failure of the specimen, the deformation is only accommodated by the elastic deformation of B19' martensite without any evidence of plastic deformation. Furthermore, all SIM transformations in this alloy are fully reversible regardless of the applied strain value. The precise knowledge of deformation sequences of all the alloys investigated will be of great importance in explaining and analyzing their fatigue performance.

### **4.3. Fatigue properties**

Fatigue tests allowed to evaluate the durability of alloys subjected to large-strain cyclic loading. All alloys can be cycled at 0.5% of applied strain without failure, since only elastic deformation of austenite is involved at this level of deformation. However, at larger applied strains, the ST metastable  $\beta$  titanium alloys studied have greater durability than the NiTi alloy (Fig. 8). It also

appears that superelasticity is significantly degraded during cycles as shown by the increase of residual strain with cycles (Fig. 9 and 10). This degradation is rapid during the first cycles for all alloys and then mainly stabilizes, except for the Ti2448 ST alloy for which the superelasticity continuously decreases continuously throughout the cycling tests.

NiTi alloy shows an almost constant number of cycles to failure for all applied strains, except 0.5%. This means that the fatigue life is mainly influenced by the occurrence of SIM transformation, regardless of the level of applied strain for the tested conditions. The SIM transformation then appears to be highly detrimental to the fatigue performance in NiTi alloy. It can also be seen that the number of cycles to failure at 1% strain is slightly lower than that measured at higher strains. Given *in situ* SXR D observations (Fig. 5c), this strain level corresponds to the onset of the B2-R SIM transformation. It is then likely that the presence of R phase generates a greater accumulation of fatigue damage than B19' phase, thereby accelerating the deterioration of NiTi alloy.

The Beta III AR alloy shows fairly conventional behavior with low fatigue resistance at high applied strain. Since reversible SIM transformation occurs moderately in this alloy (Fig. 5b), deformation is mainly accommodated by plastic deformation mechanisms above 2% of applied strain, which explains the short fatigue life at high strains. However, both Beta III ST and Ti2448 ST alloys show much greater fatigue resistance than of NiTi and Beta III AR alloys at large applied strains. The fatigue life of ST alloys is almost constant in the range of 1% to 3% strain. This phenomenon, which is also observed in NiTi alloy, seems to be related to the fact that SIM transformation is the dominant deformation mechanism in this strain range. Therefore, fatigue life seems to be only determined by the SIM transformation when this mechanism is activated in both NiTi and metastable  $\beta$  titanium superelastic alloys.

As mentioned above, alloys in which the SIM transformation has a significant contribution on recoverable strain show an important increase of residual strain during cycles. This

phenomenon, known in the literature as "transformation ratcheting" [38,58], is due to the accumulation of residual inelastic strain and to the incomplete reverse transformation from martensite to austenite, the latter leading to the loss of superelasticity (functional fatigue). In NiTi alloys, this accumulation of deformation is attributed to microplastic deformation induced by repeated SIM transformations [31,38,59]. This microplasticity can occur at low stresses, below the elastic limit, and is due to stress accumulation at the austenite/martensite interfaces that facilitates dislocation nucleation, while the applied stress is less than the critical stress for slip activation. Moreover, during mechanical cycling, the presence of such dislocations promotes the development of SIM transformation during further cycles, leading to a decrease of SIM transformation stress and hysteresis area [60], as observed in the present study (Fig. 9d and 10d). A recent study attributes the origin of functional fatigue in NiTi alloys to a symmetry-dictated non-phase-transformation pathway leading to the generation of dislocations in austenite [32]. This functional fatigue is also observed in the present study for metastable  $\beta$  titanium alloys with an increase in residual strain and a decrease in maximum stress with cycles (Fig. 9 and 10). Some recent studies on cyclic stability of metastable  $\beta$  titanium alloys have also attributed the accumulation of residual strain to microplastic deformation induced by SIM transformation [40,61].

Fatigue behavior of metastable  $\beta$  titanium alloys has been mostly studied in Ti-29Nb-13Ta-4,6Zr (TNTZ) [62,63] and Ti2448 alloys [64] with stress-controlled fatigue tests using a stress ratio  $R = 0.1$ . Under these conditions,  $\beta$  titanium alloys exhibit fatigue resistance similar to that of commercial aerospace Ti-6Al-4V ELI and Ti-6Al-7Nb alloys. However, these stress-controlled tests are very different from those performed in the present study. Strain-controlled fatigue tests have only been previously reported on the Ti2448 alloy [64]. Although this alloy was tested in hot-forged condition instead of ST condition in our present study, the reported fatigue life is almost the same. This suggests that fatigue properties are mainly limited by the

microplasticity induced by repeated SIM transformation rather than by the initial microstructural state. It has also been shown that the rotating bending fatigue performance of a metastable  $\beta$  titanium alloy is at least as good as that of NiTi alloys [65].

An important difference between NiTi and metastable  $\beta$  alloys lies in fatigue failure. For NiTi alloy, once the cyclic response is stabilized, no significant change in stress or residual strain is observed prior to failure (Fig. 9d). This sudden failure is not observed in ductile alloys, which show a significant evolution of mechanical response prior to failure, as it is the case of metastable  $\beta$  alloys that show a significant softening before failure (Fig. 9b and 9c). This behavior may allow the anticipation of fatigue failure in metastable  $\beta$  titanium alloys, which is an advantage compared to NiTi alloys that fail suddenly without any possible anticipation.

Finally, the number of cycles to failure observed in Beta III ST alloys is more than twice that of NiTi alloy and that of Ti2448 ST about five times higher, especially for large applied strains. These alloys are then promising candidates for the production of devices working at high deformation. Ti2448 ST alloy shows the best performance in the present study while it exhibits a continuous accumulation of residual strain and a significant decrease in superelasticity during the cycles. As discussed above, these phenomena are due to microplastic deformation generated at the austenite/martensite interfaces during cycling. Better fatigue properties are then attributed to a less detrimental SIM transformation in  $\beta$  titanium alloys than in NiTi alloys that can be explained by its strong localization in NiTi alloys. Indeed, SIM transformation occurs homogeneously in  $\beta$  titanium alloys, while it only occurs in some localized Lüders bands in NiTi alloys. This strong localization causes an inhomogeneous distribution of strain between the austenite and the newly formed martensite [31,33,66], leading to crack nucleation in Lüders bands or at their interface with the austenite during fatigue tests [66]. The non-localization of SIM transformation in  $\beta$  titanium alloys thus seems to “dilute” the effects of harmful defects generated at the austenite/martensite interfaces during cycling. Another improvement of fatigue

performance can also be expected by designing alloys with better compatibility between austenite and martensite, leading to fewer microplastic deformations at these interfaces and thus better stability of superelasticity and longer fatigue life.

## 5. Conclusion

*In situ* tensile tests were performed under X-ray synchrotron radiation to characterize SIM transformations in NiTi and metastable  $\beta$  titanium alloys. The fatigue performance of these superelastic alloys was determined from strain-controlled fatigue tests. From these results, the following conclusions can be drawn.

1. SIM transformation: The investigated metastable  $\beta$  titanium alloys show a direct SIM transformation between  $\beta$  austenitic and  $\alpha''$  martensitic phases. In the Beta III alloy, the SIM transformation takes place in the plastic domain, in contrast to the Ti2448 ST alloy which shows a classical superelastic behavior. In the NiTi alloy, the intermediate B2-R SIM transformation occurs before the B2-B19' SIM transformation. The SIM transformations of NiTi alloy are almost completely reversible and no plastic deformation is observed until failure, whereas metastable  $\beta$  titanium alloys show plastic deformation and stabilization of martensite before failure.
2. Functional fatigue: All alloys show a decrease in superelasticity and hysteresis area with cycling. In NiTi alloy, the mechanical response stabilizes after hundreds of cycles but the fatigue failure occurs without warning, whereas the mechanical response of metastable  $\beta$  alloys evolves continuously and shows significant softening before failure. Beta III ST and Ti2448 ST alloys show much better fatigue resistance than NiTi alloy.
3. Effect of SIM transformation on fatigue properties: For all alloys, the fatigue life is almost constant once SIM transformation becomes the main deformation mechanism, indicating its strong effect on fatigue properties. SIM transformation is shown to be more detrimental in NiTi

alloy than in metastable  $\beta$  titanium alloys. Furthermore, B2-R SIM transformation is slightly more detrimental than B2-B19' SIM transformation in NiTi. The highly localized SIM transformation in NiTi alloys results in a high concentration of detrimental defects that promote crack nucleation. In contrast,  $\beta$  titanium alloys exhibit homogeneous nucleation of the SIM transformation, which reduces the detrimental effects of defects generated at austenite/martensite interfaces during cycling, resulting in better fatigue properties. Finally, the combination of excellent durability and ductile fatigue failure makes metastable  $\beta$  titanium alloys competitive materials for applications requiring large strain fatigue performance.

### **Acknowledgment**

The authors thank the European Synchrotron Radiation Facility for providing of synchrotron radiation facilities and would like to thank the ID 22 beamline team. The authors also acknowledge the THEMIS platform of the University of Rennes for providing access to TEM facilities.

### **Data availability**

Data will be made available on request.

### **References**

- [1] M. Maroof, R. Sujithra, R.P. Tewari, Superelastic and shape memory equi-atomic nickel-titanium (Ni-Ti) alloy in dentistry: A systematic review, *Mater. Today Com.* 33 (2022) 104352. <https://doi.org/10.1016/j.mtcomm.2022.104352>.
- [2] X. Wang, J.J. Noël, I.O. Wallinder, Y.S. Hedberg, Metal bioaccessibility in synthetic body fluids – A way to consider positive and negative alloying effects in hazard

- assessments, *Mater. Des.* 198 (2021) 109393.  
<https://doi.org/10.1016/j.matdes.2020.109393>.
- [3] P. Močnik, T. Kosec, A Critical Appraisal of the Use and Properties of Nickel-Titanium Dental Alloys, *Mater.* 14 (2021) 7859. <https://doi.org/10.3390/ma14247859>.
- [4] S. Nagaraja, R. Brown, D. Saylor, A. Undisz, Oxide Layer Formation, Corrosion, and Biocompatibility of Nitinol Cardiovascular Devices. *Shap. Mem. Superelast.* 8 (2022) 45–63. <https://doi.org/10.1007/s40830-022-00365-2>.
- [5] D. Kalita, Ł. Rogal, K. Berent, A. Góral, J. Dutkiewicz, Effect of Mo and Ta on the Mechanical and Superelastic Properties of Ti-Nb Alloys Prepared by Mechanical Alloying and Spark Plasma Sintering. *Mater.* 14 (2021) 2619. <https://doi.org/10.3390/ma14102619>.
- [6] S. Li, W.-T. Lee, J.-T. Yeom, J.G. Kim, J.S. Oh, T. Lee, Y. Liu, T.-H. Nam, Towards bone-like elastic modulus in TiNbSn alloys with large recovery strain for biomedical applications, *J. Alloy. Compd.* 925 (2022) 166724. <https://doi.org/10.1016/j.jallcom.2022.166724>.
- [7] E.M. Hildyard, L.D. Connor, N.L. Church, T.E. Whitfield, N. Martin, D. Rugg, H.J. Stone, N.G. Jones, On the role of internal stresses on the superelastic behaviour of Ti-24Nb (at.%), *Acta Mater.* 237 (2022) 118161. <https://doi.org/10.1016/j.actamat.2022.118161>.
- [8] E. Bertrand, P. Castany, Y. Yang, E. Menou, L. Couturier, T. Gloriant, Origin of  $\{112\} \langle 111 \rangle$  antitwinning in a Ti-24Nb-4Zr-8Sn superelastic single crystal, *J. Mater. Sci.* 57 (2022) 7327-7342. <https://doi.org/10.1007/s10853-022-07086-y>
- [9] N.L. Church, L.D. Connor, N.G. Jones, The effect of sample size on the microstructure and mechanical properties of Ti2448 (Ti-24Nb-4Zr-8Sn wt%), *Scripta Mater.* 222 (2023) 115035. <https://doi.org/10.1016/j.scriptamat.2022.115035>.

- [10] S. Pilz, A. Hariharan, F. Günther, M. Zimmermann, A. Gebert, Influence of isothermal omega precipitation aging on deformation mechanisms and mechanical properties of a  $\beta$ -type Ti-Nb alloy, *J. Alloy. Compd.* 930 (2023) 167309. <https://doi.org/10.1016/j.jallcom.2022.167309>.
- [11] J. Stráský, D. Preisler, H. Seiner, L. Bodnárová, M. Janovská, T. Košutová, P. Hrcuba, K. Šalata, K. Halmešová, J. Džugan, M. Janeček, Achieving high strength and low elastic modulus in interstitial biomedical Ti-Nb-Zr-O alloys through compositional optimization, *Mater. Sci. Eng. A* 839 (2022) 142833. <https://doi.org/10.1016/j.msea.2022.142833>.
- [12] J. Wang, W. Xiao, L. Ren, Y. Fu, C. Ma, The roles of oxygen content on microstructural transformation, mechanical properties and corrosion resistance of Ti-Nb-based biomedical alloys with different  $\beta$  stabilities, *Mater. Charac.* 176 (2021) 111122. <https://doi.org/10.1016/j.matchar.2021.111122>.
- [13] Y. Yang, P. Castany, M. Cornen, F. Prima, S.J. Li, Y.L. Hao, T. Gloriant, Characterization of the martensitic transformation in the superelastic Ti-24Nb-4Zr-8Sn alloy by in situ synchrotron X-ray diffraction and dynamic mechanical analysis, *Acta Mater.* 88 (2015) 25–33. <https://doi.org/10.1016/j.actamat.2015.01.039>.
- [14] N.L. Church, N.G. Jones, The influence of stress on subsequent superelastic behaviour in Ti2448 (Ti-24Nb-4Zr-8Sn, wt%), *Mater. Sci. Eng. A* 833 (2022) 142530. <https://doi.org/10.1016/j.msea.2021.142530>.
- [15] X. Li, T. Chen, J. Hu, S. Li, Q. Zou, Y. Li, N. Jiang, H. Li, J. Li, Modified surface morphology of a novel Ti-24Nb-4Zr-7.9Sn titanium alloy via anodic oxidation for enhanced interfacial biocompatibility and osseointegration, *Colloids Surf. B Biointerfaces* 144 (2016) 265–275. <https://doi.org/10.1016/j.colsurfb.2016.04.020>.
- [16] M. Tahara, H.Y. Kim, H. Hosoda, S. Miyazaki, Cyclic deformation behavior of a Ti-26

- at.% Nb alloy, *Acta Mater.* 57 (2009) 2461–2469.  
<https://doi.org/10.1016/j.actamat.2009.01.037>.
- [17] W.-T. Chiu, K. Wakabayashi, A. Umise, M. Tahara, T. Inamura, H. Hosoda, Investigations of mechanical properties and deformation behaviors of the Cr modified Ti–Au shape memory alloys, *J. Alloy. Compd.* 897 (2022) 163134, <https://doi.org/10.1016/j.jallcom.2021.163134>.
- [18] B. Qian, S.A. Mantri, S. Dasari, J. Zhang, L. Liliensten, F. Sun, P. Vermaut, R. Banerjee, F. Prima, Mechanisms underlying enhanced strength-ductility combinations in TRIP/TWIP Ti-12Mo alloy engineered via isothermal omega precipitation, *Acta Mater.* 245 (2023) 118619. <https://doi.org/10.1016/j.actamat.2022.118619>.
- [19] B. Qian, J. Zhang, Y. Fu, F. Sun, Y. Wu, J. Cheng, P. vermaut, F. Prima, In-situ microstructural investigations of the TRIP-to-TWIP evolution in Ti-Mo-Zr alloys as a function of Zr concentration, *J. Mater. Sci. Tech.* 65 (2021) 228-237. <http://doi.org/10.1016/j.jmst.2020.04.078>.
- [20] J.J. Gao, P. Castany, T. Gloriant, Synthesis and characterization of a new TiZrHfNbTaSn high-entropy alloy exhibiting superelastic behavior, *Scripta Mater.* 198 (2021) 113824. <https://doi.org/10.1016/j.scriptamat.2021.113824>.
- [21] J.J. Gao, P. Castany, T. Gloriant, Complex multi-step martensitic twinning process during plastic deformation of the superelastic Ti-20Zr-3Mo-3Sn alloy, *Acta Mater.* 136 (2022) 118140. <https://doi.org/10.1016/j.actamat.2022.118140>.
- [22] M.F. Ijaz, D. Laillé, L. Héraud, D.M. Gordin, P. Castany, T. Gloriant, Design of a novel superelastic Ti-23Hf-3Mo-4Sn biomedical alloy combining low modulus, high strength and large recovery strain, *Mater. Lett.* 177 (2016) 39–41. <https://doi.org/10.1016/j.matlet.2016.04.184>.
- [23] M.F. Ijaz, L. Héraud, P. Castany, I. Thibon, T. Gloriant, Superelastic Behavior of

- Biomedical Metallic Alloys, *Metall. Mater. Trans. A* 51 (2020) 3733–3741.  
<https://doi.org/10.1007/s11661-020-05840-y>.
- [24] P. Laheurte, A. Eberhardt, M.J. Philippe, Influence of the microstructure on the pseudoelasticity of a metastable beta titanium alloy, *Mater. Sci. Eng. A* 396 (2005) 223–230. <https://doi.org/10.1016/j.msea.2005.01.022>.
- [25] V. Sheremetyev, S. Dubinskiy, A. Kudryashova, S. Prokoshkin, V. Brailovski, In situ XRD study of stress- and cooling-induced martensitic transformations in ultrafine- and nano-grained superelastic Ti-18Zr-14Nb alloy, *J. Alloy. Compd.* 902 (2022) 163704. <https://doi.org/10.1016/j.jallcom.2022.163704>.
- [26] L. Héraud, P. Castany, D. Lailllé, T. Gloriant, In situ synchrotron X-ray diffraction of the martensitic transformation in superelastic Ti-27Nb and NiTi alloys: A comparative study, *Mater. Today Proc.* 2 (2015) S917–S920. <https://doi.org/10.1016/j.matpr.2015.07.431>.
- [27] P. Castany, A. Ramarolahy, F. Prima, P. Laheurte, C. Curfs, T. Gloriant, In situ synchrotron X-ray diffraction study of the martensitic transformation in superelastic Ti-24Nb-0.5N and Ti-24Nb-0.5O alloys, *Acta Mater.* 88 (2015) 102–111. <https://doi.org/10.1016/j.actamat.2015.01.014>.
- [28] S. Guo, W. Ding, H. Zhang, W. Lu, G. Liu, H. Liu, X. Cheng, X. Zhao, Mechanisms of near-linear elastic deformation behavior in a binary metastable  $\beta$ -type Ti-Nb alloy with large recoverable strain, *Mater. Charac.* 187 (2022) 111858. <https://doi.org/10.1016/j.matchar.2022.111858>.
- [29] T.R. Finlayson, The Contributions by Kazuhiro Otsuka to “Shape Memory and Superelasticity”: A Review, *Shap. Mem. Superelast. in press* (2023). <https://doi.org/10.1007/s40830-022-00406-w>.
- [30] W.S. Choi, E.L. Pang, W.-S. Ko, H. Jun, H.J. Bong, C. Kirchlechner, D. Raabe, P.-P. Choi, Orientation-dependent plastic deformation mechanisms and competition with

- stress-induced phase transformation in microscale NiTi, *Acta Mater.* 208 (2021) 116731. <https://doi.org/10.1016/j.actamat.2021.116731>.
- [31] K. Nargatti, S. Ahankari, Advances in enhancing structural and functional fatigue resistance of superelastic NiTi shape memory alloy: A Review. *J. Intell. Mater. Syst. Struct.* 33 (2022) 503-531. <https://doi.org/10.1177/1045389X211023>.
- [32] Y. Gao, L. Casalena, M.L. Bowers, R.D. Noebe, M.J. Mills, Y. Wang, An origin of functional fatigue of shape memory alloys, *Acta Mater.* 126 (2017) 389–400. <https://doi.org/10.1016/j.actamat.2017.01.001>.
- [33] E. Alarcon, L. Heller, S.A. Chirani, P. Šittner, J. Kopeček, L. Saint-Sulpice, S. Calloch, Fatigue performance of superelastic NiTi near stress-induced martensitic transformation, *Int. J. Fatigue* 95 (2017) 76–89. <https://doi.org/10.1016/j.ijfatigue.2016.10.005>.
- [34] A. Zanza, M. Seracchiani, R. Reda, D. Di Nardo, G. Gambarini, L. Testarelli, Role of the crystallographic phase of NiTi rotary instruments in determining their torsional resistance during different bending conditions, *Mater.* 14 (2021) 6324. <https://doi.org/10.3390/ma14216324>.
- [35] L.G. Malito, , P.L. Briant, , M.L. Bowers, S. Easley, J.E. Schaffer, B. James, Fatigue, Fracture, and Crack Arrest from Bending Induced Pre-strain in Superelastic Nitinol, *Shap. Mem. Superelast.* 8 (2022) 129–141. <https://doi.org/10.1007/s40830-022-00375-0>.
- [36] J.D. Weaver, G.M. Sena, K.I. Aycock, A. Roiko, W. M. Falk, S. Sivan, B. T. Berg Rotary Bend Fatigue of Nitinol to One Billion Cycles, *Shap. Mem. Superelast.* *in press* (2023). <https://doi.org/10.1007/s40830-022-00409-7>.
- [37] R. Sidharth, A.S.K. Mohammed, H. Sehitoglu, Functional Fatigue of NiTi Shape Memory Alloy: Effect of Loading Frequency and Source of Residual Strains. *Shap. Mem. Superelast.* 8 (2022) 394–412. <https://doi.org/10.1007/s40830-022-00397-8>.

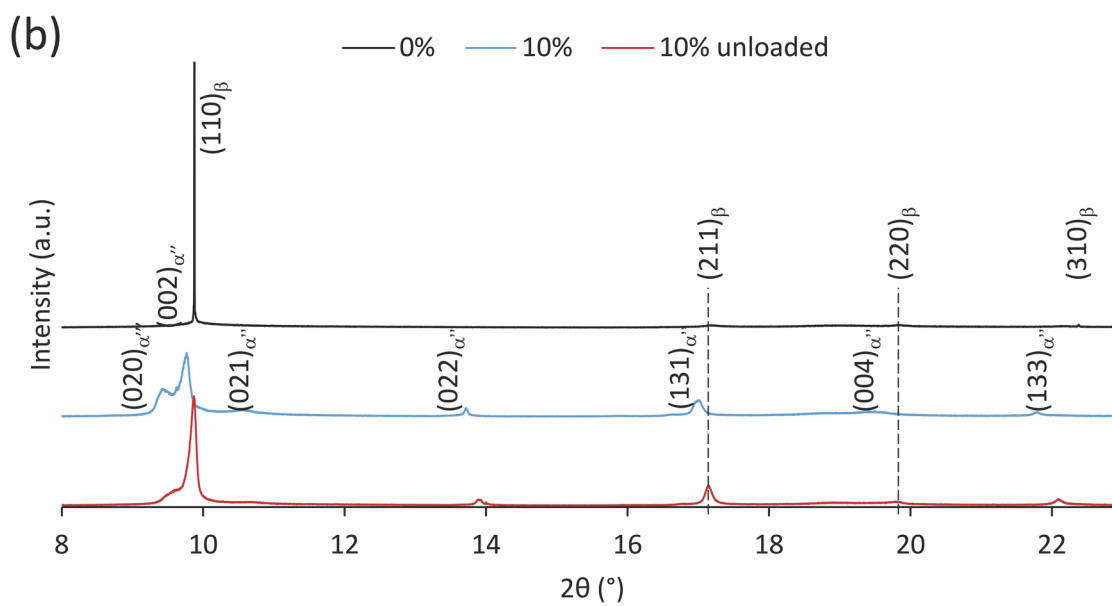
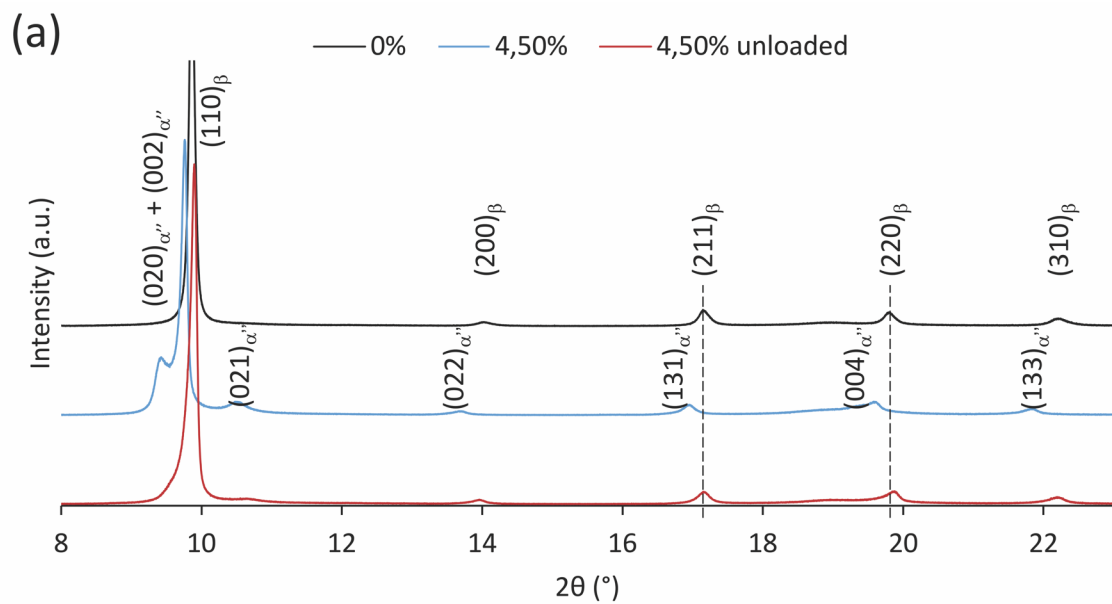
- [38] C. Maletta, E. Sgambitterra, F. Furgiuele, R. Casati, A. Tuissi, Fatigue properties of a pseudoelastic NiTi alloy: Strain ratcheting and hysteresis under cyclic tensile loading, *Int. J. Fatigue* 66 (2014) 78–85. <https://doi.org/10.1016/j.ijfatigue.2014.03.011>.
- [39] A.R. Pelton, B.T. Berg, P. Saffari, A. P. Stebner, A. N. Bucsek, Pre-strain and Mean Strain Effects on the Fatigue Behavior of Superelastic Nitinol Medical Devices. *Shap. Mem. Superelast.* 8 (2022) 64–84. <https://doi.org/10.1007/s40830-022-00377-y>.
- [40] V. Sheremetyev, V. Brailovski, S. Prokoshkin, K. Inaekyan, S. Dubinskiy, Functional fatigue behavior of superelastic beta Ti-22Nb-6Zr(at%) alloy for load-bearing biomedical applications., *Mater. Sci. Eng. C* 58 (2016) 935–44. <https://doi.org/10.1016/j.msec.2015.09.060>.
- [41] X. Song, L. Wang, M. Niinomi, M. Nakai, Y. Liu, Fatigue characteristics of a biomedical  $\beta$ -type titanium alloy with titanium boride, *Mater. Sci. Eng. A* 640 (2015) 154–164. <https://doi.org/10.1016/j.msea.2015.05.078>.
- [42] L. Campanelli, A review on the recent advances concerning the fatigue performance of titanium alloys for orthopedic applications, *J. Mater. Res.* 36 (2021) 151-165. <https://doi.org/10.1557/s43578-020-00087-0>.
- [43] Z. Moumni, A. Van Herpen, P. Riberty, Fatigue analysis of shape memory alloys: energy approach, *Smart Mater. Struct.* 14 (2005) S287–S292. <https://doi.org/10.1088/0964-1726/14/5/017>.
- [44] M.J. Blackburn, J.A. Feeney, Stress-induced transformations in Ti-Mo alloys, *J. Inst. Met.* 99 (1970) 132-134.
- [45] S. Hanada, O. Izumi, Correlation of tensile properties, deformation modes, and phase stability in commercial  $\beta$ -phase titanium alloys, *Metall. Trans. A* 18 (1987) 265–271. <https://doi.org/10.1007/BF02825707>.
- [46] M. González, J. Peña, F.J. Gil, J.M. Manero, Low modulus Ti-Nb-Hf alloy for

- biomedical applications, *Mater. Sci. Eng. C* 42 (2014) 691–695.  
<https://doi.org/10.1016/j.msec.2014.06.010>.
- [47] M. Niinomi, Mechanical biocompatibilities of titanium alloys for biomedical applications, *J. Mech. Behav. Biomed. Mater.* 1 (2008) 30–42.  
<https://doi.org/10.1016/j.jmbbm.2007.07.001>.
- [48] N.J. Bechle, S. Kyriakides, Localization in NiTi tubes under bending, *Int. J. Solids Struct.* 51 (2014) 967–980. <https://doi.org/10.1016/j.ijsolstr.2013.11.023>.
- [49] W.W. Schmahl, J. Khalil-Allafi, B. Hasse, M. Wagner, A. Heckmann, C. Somsen, Investigation of the phase evolution in a super-elastic NiTi shape memory alloy (50.7 at.%Ni) under extensional load with synchrotron radiation, *Mater. Sci. Eng. A* 378 (2004) 81–85. <https://doi.org/10.1016/j.msea.2003.11.081>.
- [50] B.S. Shariat, S. Bakhtiari, H. Yang, Y. Liu, Controlled initiation and propagation of stress-induced martensitic transformation in functionally graded NiTi, *J. Alloy. Compd.* 851 (2021) 156103. <https://doi.org/10.1016/j.jallcom.2020.156103>.
- [51] T.W. Duerig, K. Bhattacharya, The Influence of the R-Phase on the Superelastic Behavior of NiTi, *Shape Mem. Superelast.* 1 (2015) 153–161.  
<https://doi.org/10.1007/s40830-015-0013-4>.
- [52] F. Sun, J.Y. Zhang, M. Marteleur, T. Gloriant, P. Vermaut, D. Laillé, P. Castany, C. Curfs, P.J. Jacques, F. Prima, Investigation of early stage deformation mechanisms in a metastable  $\beta$  titanium alloy showing combined twinning-induced plasticity and transformation-induced plasticity effects, *Acta Mater.* 61 (2013) 6406–6417.  
<https://doi.org/10.1016/j.actamat.2013.07.019>.
- [53] P. Castany, T. Gloriant, F. Sun, F. Prima, Design of strain-transformable titanium alloys, *Comptes Rendus Phys.* 19 (2018) 710–720. <https://doi.org/10.1016/j.crhy.2018.10.004>.
- [54] E. Bertrand, P. Castany, Y. Yang, E. Menou, T. Gloriant, Deformation twinning in the

- full- $\alpha'$  martensitic Ti–25Ta–20Nb shape memory alloy, *Acta Mater.* 105 (2016) 94–103.  
<https://doi.org/10.1016/j.actamat.2015.12.001>.
- [55] M.J. Lai, C.C. Tasan, D. Raabe, On the mechanism of {332} twinning in metastable  $\beta$  titanium alloys, *Acta Mater.* 111 (2016) 173–186.  
<https://doi.org/10.1016/j.actamat.2016.03.040>.
- [56] L. Lilensten, Y. Danard, C. Brozek, S. Mantri, P. Castany, T. Gloriant, P. Vermaut, F. Sun, R. Banerjee, F. Prima, On the heterogeneous nature of deformation in a strain-transformable beta metastable Ti-V-Cr-Al alloy, *Acta Mater.* 162 (2019) 268–276.  
<https://doi.org/10.1016/j.actamat.2018.10.003>.
- [57] S. Cai, M.R. Daymond, Y. Ren, J.E. Schaffer, Evolution of lattice strain and phase transformation of  $\beta$  III Ti alloy during room temperature cyclic tension, *Acta Mater.* 61 (2013) 6830–6842. <https://doi.org/10.1016/j.actamat.2013.07.062>.
- [58] G. Kang, Q. Kan, L. Qian, Y. Liu, Ratchetting deformation of super-elastic and shape-memory NiTi alloys, *Mech. Mater.* 41 (2009) 139–153.  
<https://doi.org/10.1016/j.mechmat.2008.09.001>.
- [59] M. Abdel-Karim, Shakedown of complex structures according to various hardening rules, *Int. J. Press. Vessel. Pip.* 82 (2005) 427–458.  
<https://doi.org/10.1016/j.ijpvp.2005.01.007>.
- [60] S.W. Robertson, A.R. Pelton, R.O. Ritchie, Mechanical fatigue and fracture of Nitinol, *Int. Mater. Rev.* 57 (2012) 1–37. <https://doi.org/10.1179/1743280411Y.0000000009>.
- [61] J. Coakley, K.M. Rahman, V.A. Vorontsov, M. Ohnuma, D. Dye, Effect of precipitation on mechanical properties in the  $\beta$ -Ti alloy Ti–24Nb–4Zr–8Sn, *Mater. Sci. Eng. A* 655 (2016) 399–407. <https://doi.org/10.1016/j.msea.2015.12.024>.
- [62] T. Akahori, M. Niinomi, A. Noda, H. Toda, F. Hisao, O. Michiharu, Effect of Aging Treatment on Mechanical Properties of Ti-29Nb-13Ta-4.6 Zr Alloy for Biomedical

- Applications, *J. Japan Inst. Met.* 70 (2006) 295–303.
- [63] M. Niinomi, Fatigue characteristics of metallic biomaterials, *Int. J. Fatigue* 29 (2007) 992–1000. <https://doi.org/10.1016/j.ijfatigue.2006.09.021>.
- [64] S.J. Li, T.C. Cui, Y.L. Hao, R. Yang, Fatigue properties of a metastable  $\beta$ -type titanium alloy with reversible phase transformation, *Acta Biomater.* 4 (2008) 305–317. <https://doi.org/10.1016/j.actbio.2007.09.009>.
- [65] J. Guillem-Martí, C. Herranz-Díez, J.E. Shaffer, F.J. Gil, J.M. Manero, Mechanical and microstructural characterization of new nickel-free low modulus  $\beta$ -type titanium wires during thermomechanical treatments, *Mater. Sci. Eng. A* 636 (2015) 507–515. <https://doi.org/10.1016/j.msea.2015.03.060>.
- [66] L. Zheng, Y. He, Z. Moumni, Effects of Lüders-like bands on NiTi fatigue behaviors, *Int. J. Sol. Struct.* 83 (2016) 28–44. <https://doi.org/10.1016/j.ijsolstr.2015.12.021>.

## Supplementary material



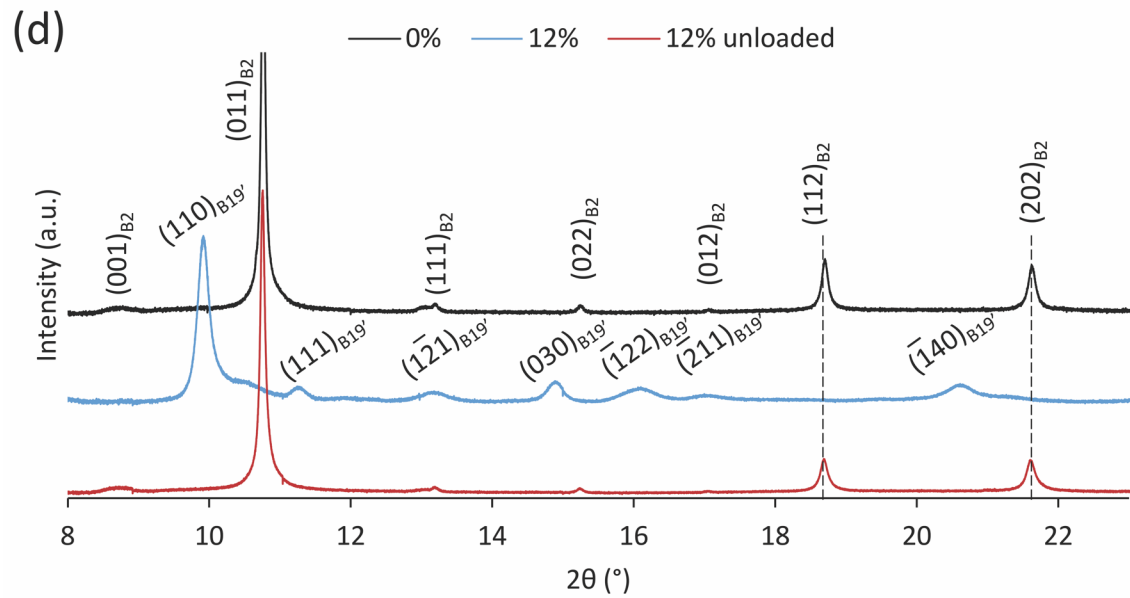
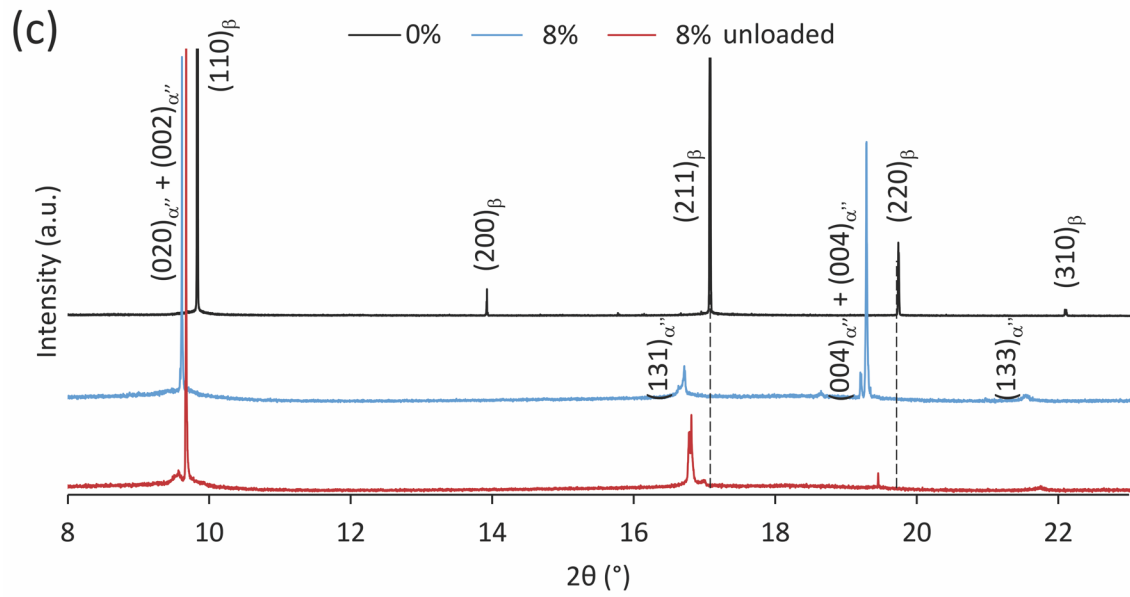


Fig. S1 - Full SAXRD patterns of Beta III AR (a), Beta III ST (b), Ti2448 ST (c) and NiTi (d) alloys acquired before starting the tensile test (top), under loading at 4.5%, 10%, 8% and 12% of applied strain respectively and after the end of the entire cyclic tensile test (bottom).